https://doi.org/10.5194/egusphere-2026-6116
Preprint. Discussion started: 5 November 2026
© Author(s) 2026. CC BY 4.0 License.

All-weather lake-ice phenology from Sentinel-1 and reanalysis thermodynamics: a validated, transferable method applied to 131 Adirondack lakes

Marzi Azarderakhsh[1], Samuel E. Tuttle[2], Madhushree Munsi[3], Stacy A. McNulty[4], Michale J. Glennon[5], Brendan Wiltse[6], Peter B. McIntyre[7], and Kevin C. Rose[8,9]

[1]Department of Construction Management and Civil Engineering Technology, New York City College of Technology, City University of New York, Brooklyn, NY, USA

[2]Department of Earth and Environmental Sciences, Syracuse University, Syracuse, NY, USA

[3]Darrin Fresh Water Institute, Rensselaer Polytechnic Institute, Troy, NY, USA

[4]Adirondack Ecological Center, Department of Environmental Biology, State University of New York College of Environmental Science and Forestry, Newcomb, NY, USA

[5]Adirondack Watershed Institute, Paul Smith's College, Paul Smiths, NY, USA

[6]Lake George Association, Lake George, NY, USA

[7]Department of Ecology and Evolutionary Biology, Cornell University, Ithaca, NY, USA

[8]Department of Biological Sciences, Rensselaer Polytechnic Institute, Troy, NY, USA

[9]Department of Civil and Environmental Engineering, Rensselaer Polytechnic Institute, Troy, NY, USA

Correspondence: Marzi Azarderakhsh (MaAzarderakhsh@citytech.cuny.edu)

Abstract

Lake ice phenology is a sensitive and physically interpretable indicator of climate change, but observer records exist for only a small and shrinking subset of lakes, and optical satellite methods are limited by cloud in precisely the season when freeze-up and break-up occur. We present a method that estimates freeze-up and break-up dates by combining Sentinel-1 C-band backscatter with gridded reanalysis thermodynamics in a single probabilistic model. Per-scene radar features, cumulative freezing and thawing degree-days, seasonal harmonics and static lake morphometry enter a ridge logistic regression model that returns the probability of ice for each

https://doi.org/10.5194/egusphere-2026-6116
Preprint. Discussion started: 5 November 2026
© Author(s) 2026. CC BY 4.0 License.

scene. A two-state hidden Markov model with degree-day-gated transitions then converts each season's probability sequence into freeze-up and break-up dates, each with a resolution bound of half the revisit interval that brackets it. Under leave-one-lake-out cross-validation across 13 lakes and 79 lake-seasons, the method resolves freeze-up to a mean absolute error of 11.5 d and break-up to 8.3 d, against 36.1 d and 23.4 d for a fixed-threshold baseline that additionally fails to resolve break-up in 89 % of seasons. Withholding each information source in turn shows that the radar contribution is concentrated at freeze-up, where it reduces error by 4.6 d, and is negligible at break-up, which cumulative thawing degree-days already constrain. Combining the two sources also suppresses false ice detection: a meteorology-only model declares ice in all four documented no-freeze winters on Lake George and the fused model in one. Applying the developed model to 131 Adirondack lakes over ten winters yields 1,310 lake-season records with a resolution bound attached to every event, recovering an elevation gradient of 6.0 d per 100 m and a 36 d difference in median ice duration between the coldest and warmest winters. Because the method requires no local observations and no per-lake calibration, it provides a consistent baseline for regions where ice records are absent, and offers a route to extending ice-phenology monitoring to the large majority of lakes that have never been observed.

1 Introduction

Lake ice is among the most sensitive and most legible indicators of climate change. The dates on which a lake freezes and clears integrate air temperature over weeks to months, and the resulting record is a physically interpretable quantity that local and community observers have been able to record for centuries. Some of the longest instrumental environmental records in existence are lake-ice records, and they show coherent hemispheric change: freeze-up has moved later and break-up earlier across the Northern Hemisphere since the mid-nineteenth century (Magnuson et al., 2000; Benson et al., 2000; Duguay et al., 2006; L'Abée-Lund et al., 2021; Sharma et al., 2022). More recent assessments find that tens of thousands of lakes are now at risk of intermittent winter ice cover, with consequences for the ecosystem services that ice supports (Sharma et al., 2019).

Ice cover also governs lake function directly. It controls the light and gas exchange across the water surface, sets the timing of spring mixing, and determines the duration of the under-ice period that structures winter ecology (Kirillin et al., 2012; Hampton et al., 2017). Changes in its

https://doi.org/10.5194/egusphere-2026-6116
Preprint. Discussion started: 5 November 2026
© Author(s) 2026. CC BY 4.0 License.

timing propagate into stratification, oxygen availability and the seasonal cycle of production (Brown and Duguay, 2010; Leppäranta, 2023). Ice phenology is therefore not only a climate signal but a driver of the physical and biogeochemical behavior of the lakes themselves (Woolway et al., 2020; Leppäranta, 2023).

The principal limitation of lake-ice phenology as a climate indicator is the incomplete coverage of observational records. These exist for only a small and shrinking subset of lakes and are unevenly distributed across the landscape, clustering where people live and where lakes have communities, institutions, or long recreational traditions (Benson et al., 2000; Sharma et al., 2022). The great majority of lakes have never been monitored. In the Adirondack Park of northern New York State, which contains more than 11,000 lakes and ponds (Adirondack Watershed Institute, 2026a), surface waters have warmed by approximately 0.89 °C per decade over the past four decades, with the strongest warming in the shoulder seasons (Azarderakhsh et al., 2025), and the three-decade Huntington Wildlife Forest record shows that ice phenology there responds most strongly to conditions in those shoulder months (Beier et al., 2012). Ice-out has advanced across New England since 1850 (Hodgkins et al., 2002), small north-temperate lakes of the Great Lakes region now freeze later and clear earlier than they did in the early 1980s (Hewitt et al., 2018), and ice-out on Lower St. Regis Lake in the Adirondack uplands now occurs about a week earlier than it did in 1909 (Stager et al., 2022). Yet documented ice-phenology records exist for only a small number of Adirondack lakes. Most of the lakes for which this signal would be useful have no observational record.

Satellite remote sensing offers a way to close that gap, but optical and thermal sensors cannot see a lake surface through cloud, and cloud frequency in temperate forest regions is highest in the winter and shoulder-season months when freeze-up and break-up occur. The result is that optical time series are sparsest precisely when dense observations are most needed during freeze-up and break-up. This limitation has shaped the development of optical and thermal approaches to lake-ice phenology. Visible, near-infrared, and thermal infrared observations from the Advanced Very High Resolution Radiometer (AVHRR) and the Moderate Resolution Imaging Spectroradiometer (MODIS) have yielded ice dates for lakes across Canada, Europe, the Tibetan Plateau, and the northeastern United States (Latifovic and Pouliot, 2007; Kropáček et al., 2013; Weber et al., 2016; Zhang and Pavelsky, 2019). The same observations underpin global products, including

https://doi.org/10.5194/egusphere-2026-6116
Preprint. Discussion started: 5 November 2026
© Author(s) 2026. CC BY 4.0 License.

the 250 m ice-cover record of the ESA Lakes Climate Change Initiative (Carrea et al., 2023) and the Landsat-based ice-phenology estimates of Korver et al. (2024) for 1.4 million lakes. Other approaches use MODIS land-surface temperature to accumulate degree-day sums through cloud gaps rather than observing the transition directly (Skoglund et al., 2024). The same cloud limitation also restricts the number of usable scenes in optical studies of the Adirondack lakes (Azarderakhsh et al., 2025), and at the resolution of the global products the small lakes that make up most of the park's waterbodies occupy only one or a few pixels, so a method that observes small temperate lakes through winter cloud adds information that these products cannot supply.

Synthetic aperture radar (SAR) does not share this limitation. As an active microwave sensor it is independent of solar illumination and largely unaffected by cloud cover, so it acquires imagery on a fixed revisit schedule regardless of weather or time of day. The scattering contrast between open water, which acts as a specular reflector, and ice cover, which returns energy from the rough ice–water interface, makes the two states distinguishable in principle (Duguay et al., 2002; Surdu et al., 2014; Atwood et al., 2015). Five decades of work have established the physical basis for this and demonstrated it across a wide range of lake types and radar frequencies, from shallow sub-Arctic lakes to permafrost lakes and high-latitude ice regimes (Sobiech and Dierking, 2013; Antonova et al., 2016; Surdu et al., 2016; Murfitt and Duguay, 2020, 2021).

In practice, most operational applications of SAR to lake ice have relied on a threshold applied to backscatter, with ice declared when the return crosses a chosen level, whether that level is set manually, derived from an unsupervised classification of the scene histogram, or adapted per lake from the observed range of the season (Sobiech and Dierking, 2013; Antonova et al., 2016; Murfitt and Duguay, 2021). Supervised classifiers have also been trained to label ice and water in individual scenes, including deep networks applied to Sentinel-1 over Swiss lakes (Tom et al., 2020), segmentation combined with random-forest labeling of RADARSAT-2 imagery (Hoekstra et al., 2020) and machine-learning classifiers for global MODIS ice mapping (Wu et al., 2021), and Tong et al. (2024) combined high-resolution optical observations with climatological predictors to reconstruct daily ice cover on lakes of the Tibetan Plateau. These approaches classify scenes; the phenological event is then extracted from the sequence of labels, usually by a threshold or crossing rule. Threshold detection can work well on an individual lake but generalizes poorly across a heterogeneous lake population, for three reasons whose

https://doi.org/10.5194/egusphere-2026-6116
Preprint. Discussion started: 5 November 2026
© Author(s) 2026. CC BY 4.0 License.

consequences are quantified by the threshold baseline in Sect. 3.2 and which motivate the design in Sect. 2.5: the transition from open water to consolidated ice is often gradual rather than abrupt, so any threshold may be crossed late; the absolute backscatter of an ice cover varies between lakes for reasons unrelated to ice, such as differences in fetch, shoreline geometry and the proportion of shallow margins within the water mask, so a threshold that suits one lake may not necessarily work on another; and wind roughening raises the return from open water toward the level expected from ice, so a single scene cannot distinguish the two. These are not problems that can be solved by simply adjusting a threshold or tuning a parameter. Instead, they reflect the nature of the observations themselves and therefore determine the requirements of any method intended to operate automatically across many lakes.

This paper presents a framework that combines Sentinel-1 SAR observations with gridded thermodynamic information to estimate lake freeze-up and break-up without site-specific calibration. A probabilistic observation model is coupled with a thermodynamically constrained temporal model to infer event dates and their associated uncertainty. Rather than applying meteorological information as a post-processing correction, the two information sources are integrated within a single estimation framework. To our knowledge, no study has combined SAR with thermodynamic constraints in a temporal model designed to transfer across unmonitored temperate lakes.

The framework is evaluated using four complementary tests. First, leave-one-lake-out cross-validation assesses its ability to generalize to previously unmonitored lakes. Second, withholding each information source in turn quantifies the contribution of the radar and meteorological predictors. Third, the model configuration is fixed before the 2025–26 ice season, providing an independent prospective evaluation. Fourth, observations from three lakes that became available after model development provide an independent test on lakes never used in development or cross-validation.

We then apply the finalized model to 131 lakes over ten winters, producing 1,310 lake-season records with a resolution bound attached to every event for a lake population in which only a small fraction of lakes have documented ice-phenology records. Section 2 describes the data and the method, Sect. 3 the evaluation and the park-wide dataset, and Sect. 4 the implications and limitations.

https://doi.org/10.5194/egusphere-2026-6116
Preprint. Discussion started: 5 November 2026
© Author(s) 2026. CC BY 4.0 License.

2 Data and method

2.1 Study area

The Adirondack Park in northern New York State is the largest protected area in the contiguous United States, covering roughly 2.4 million ha and containing more than 11,000 lakes and ponds (Adirondack Watershed Institute, 2026a). The terrain is montane to subalpine, with elevations from about 300 m to over 1,600 m, and annual precipitation of 1,000 to 1,200 mm, much of it snow. Most waterbodies are small, shallow and hydrologically isolated, a legacy of glaciation. Winters are long and cold: over the ten study winters, December to February mean air temperature across the study lakes averaged −6.6 °C, ranging from −3.6 °C in 2023–24 to −9.3 °C in 2025–26, and season-total freezing degree-days averaged about 500 °C·d in the warmest winter and 1,000 °C·d in the coldest (Daymet, Sect. 2.3). Detailed ice records exist for only a small subset of lakes, while the great majority remain unmonitored. Regional surface-water warming in the Adirondacks has been documented previously (Azarderakhsh et al., 2025), and ice-out on Lower St. Regis Lake is now about a week earlier than it was in 1909 (Stager et al., 2022).

Two lake populations are used. The application set comprises 131 lakes within the park boundary, spanning ten ice seasons from 2016–17 to 2025–26 (Table 1; the full catalogue is given in Table S1). It was assembled in two steps: 125 lakes were selected from OpenStreetMap water polygons inside the park boundary with a surface area of at least 50 ha and regular ascending-node Sentinel-1 coverage, and the in-park validation lakes not already in that set were added, including the four below 50 ha (Lodo Pond, Military Lake, Deer Lake and Arbutus Lake), so that every in-park validation lake belongs to the application set. The 50 ha floor reflects the water-mask requirement of Sect. 2.2 rather than a sampling design, so the set is not a random sample of the park's waterbodies and over-represents lakes of 50 to 200 ha. Sixteen lakes with ice-phenology observations are available for evaluation. Thirteen are used for leave-one-lake-out cross-validation; their areas and numbers of observed seasons are listed in Table S3. Ten are located inside the park and are also part of the application set, while Cazenovia, Oneida, and Otsego lakes lie outside the park and are used only for validation. Observations from an additional three Adirondack lakes (Lake Placid, Schroon Lake, and Upper Saranac Lake) became

6

https://doi.org/10.5194/egusphere-2026-6116
Preprint. Discussion started: 5 November 2026
© Author(s) 2026. CC BY 4.0 License.

available after model development and are reserved for an independent evaluation (Sect. 2.4 and Sect. 3.4).

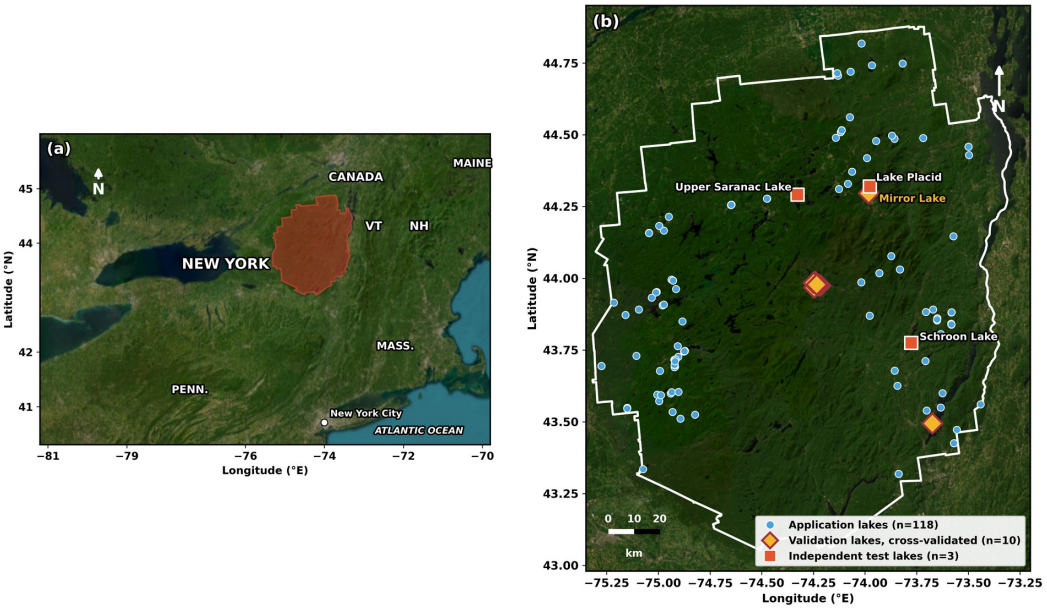
Eight of the ten in-park validation lakes are clustered within the Huntington Wildlife Forest near Newcomb (Arbutus Lake, Catlin Lake, Deer Lake, Lodo Pond, Long Pond, Military Lake, Rich Lake, and Wolf Lake) and are monitored under a single observer protocol. Only Mirror Lake and Lake George are spatially independent of that cluster, so the in-park validation sites represent three broadly independent locations rather than ten (Fig. 1). The advantage of the Huntington cluster is the consistency of its observing protocol, which removes between-observer variability from a large fraction of the validation record; its cost is that holding out one Huntington lake leaves seven similar lakes in training, which we address with a leave-one-cluster-out test in Sect. 2.10.

Area class (ha)	Lakes	Lake-seasons	Median area (ha)	Elevation range (m)
< 10	2	20	8.0	484–499
10–50	2	20	42.4	480–516
50–200	110	1100	87.6	99–676
200–1000	16	160	262.6	28–570
1000–5000	0	n/a	n/a	n/a
> 5000	1	10	11400.0	102
All	**131**	**1310**	**n/a**	**28–676**

Table 1. Lake-set summary by surface-area class for the 131-lake application set.

7

https://doi.org/10.5194/egusphere-2026-6116
Preprint. Discussion started: 5 November 2026
© Author(s) 2026. CC BY 4.0 License.



188 **Figure 1.** (a) Regional setting of the Adirondack Park within the northeastern United States. (b) The park
189 boundary with the 131 lakes of the application set: 10 lakes with observer records used in cross-validation, 3
190 lakes with independent observations used as a held-out test, and 118 application-only lakes. Cazenovia, Oneida
191 and Otsego lakes lie outside the park and are not shown. Park boundary from the Adirondack Park Agency;
192 basemap Esri World Imagery | Powered by Esri.

193 **2.2 Sentinel-1 synthetic aperture radar observations**

194 We used the Copernicus Sentinel-1 mission (Torres et al., 2012), whose C-band SAR operates at
195 a center frequency of 5.405 GHz, a wavelength of approximately 5.6 cm. Over land the mission
196 acquires by default in Interferometric Wide (IW) swath mode, imaging a 250 km swath at
197 incidence angles between approximately 29° and 46° with a single-look resolution of about 5 m
198 by 20 m. This study uses the high-resolution IW Ground Range Detected (GRD) product
199 throughout, distributed at 10 m pixel spacing, accessed through Google Earth Engine (Gorelick
200 et al., 2017), where orbit-file application, thermal-noise removal, radiometric calibration and
201 range-Doppler terrain correction have already been applied. Backscatter is expressed in decibels.

202 Sentinel-1 acquires in dual polarization over the study region, transmitting vertically and
203 receiving both vertically (VV) and horizontally (VH); we used both channels. A calm water
204 surface acts as a specular reflector and returns little energy in either channel, whereas an ice
205 cover raises the return, mainly through scattering at the rough ice–water interface, which

https://doi.org/10.5194/egusphere-2026-6116
Preprint. Discussion started: 5 November 2026
© Author(s) 2026. CC BY 4.0 License.

polarimetric studies identify as the dominant mechanism for floating freshwater ice (Atwood et al., 2015; Gunn et al., 2018), with smaller contributions from surface roughness and from volume scattering within the ice, and alters the ratio between channels (Duguay et al., 2002; Surdu et al., 2014; Murfitt and Duguay, 2021).

Only ascending-node acquisitions were used. Every scene in the archive was acquired between 22:40 and 23:00 UTC, about 18:00 local time, so restricting to one node samples the surface at a fixed time of day and avoids mixing late-afternoon conditions, when snow and ice surfaces may be wet, with the refrozen conditions of the early-morning descending passes; it also halves the spread of incidence angle and look direction across the scenes of a lake. Each lake is imaged from several ascending relative orbits, and the residual differences between them are removed by the orbit-phase centering of Sect. 2.6. Adding descending passes would densify the sampling and is discussed in Sect. 4. The nominal repeat cycle of a single Sentinel-1 satellite is 12 days. Effective revisit varies across the archive because the constellation changed over the study period: Sentinel-1B ceased operating in 2021 and the mission was formally ended in 2022, and Sentinel-1C entered service in 2025. Ascending-node revisit intervals over the study lakes are therefore typically 12 days, with longer gaps in parts of the archive. Because this interval sets the achievable precision of an event date, it is carried explicitly into the resolution bound on every event we report.

Water pixels within each lake were isolated using the Joint Research Centre Global Surface Water dataset (Pekel et al., 2016), which maps surface-water occurrence from the Landsat archive at 30 m resolution. Pixels with a water occurrence of at least 30 % were retained; for lakes where this left fewer than five pixels the threshold was relaxed to 10 % and then to 5 %. Using an occurrence-based mask rather than the lake outline alone excludes shoreline and mixed land-water pixels that would otherwise contribute a static land signal. Per-scene statistics were computed over the retained water pixels within an analysis circle of 0.64 to 2 km radius, scaled with lake area and centered on the centroid of the water mask, taking the median rather than the mean to suppress speckle. For lakes smaller than about 200 ha the circle contains most or all of the water mask, whereas for the largest lakes it samples a single patch of about 12 km², roughly a tenth of Lake George and 6 % of Oneida Lake; the consequences for break-up on large lakes are discussed in Sect. 3.1 and Sect. 4.

https://doi.org/10.5194/egusphere-2026-6116
Preprint. Discussion started: 5 November 2026
© Author(s) 2026. CC BY 4.0 License.

2.3 Meteorological and morphometric data

Air temperature was taken from Daymet Version 4, a gridded daily surface-weather product for North America at 1 km resolution (Thornton et al., 2020), and accumulated into cumulative freezing degree-days (FDD) and thawing degree-days (TDD) for each lake and season following the standard degree-day formulation (Williams, 1965; Ashton, 1986; Leppäranta, 2023). Both use daily mean air temperature with a base of 0 °C: FDD is the running sum of the departures below 0 °C from 1 October, and TDD the running sum of the departures above 0 °C from 1 January, a fixed calendar date rather than the freeze-up date, so that both quantities are defined without reference to any ice observation. Daymet omits 31 December in leap years and did not yet cover 2026 at the time of analysis; for those days, and for the 2025–26 season from 1 January 2026 onward, bias-adjusted ERA5-Land air temperature was substituted. Wind speed at each overpass was taken from ERA5-Land, the land component of the European Centre for Medium-Range Weather Forecasts (ECMWF) Reanalysis version 5 (ERA5) at approximately 9 km resolution and hourly time step (Muñoz-Sabater et al., 2021), matched to each acquisition by time and location.

Lake outlines were taken from OpenStreetMap and surface area computed from these polygons. Lake elevation was sampled from the Shuttle Radar Topography Mission digital elevation model (Farr et al., 2007) as the mean over each lake's water pixels, and maximum depth, where available, was taken from the survey records of the Adirondack Lakes Survey Corporation (Adirondack Lakes Survey Corporation, 1990). Measured depths exist for only 8 of the 131 lakes, so a binary flag records whether a measured depth was available and the remaining lakes carry a substituted value that the model can identify as such.

2.4 Ice-phenology observations

Observed freeze-up and break-up dates were compiled from three sources.

For Lake George the record has been maintained by three successive custodians: the Warren County Department of Public Works held it through 2013, the Darrin Fresh Water Institute provides assistance in monitoring, and the Lake George Association documents, compiles and publishes the series (Lake George Association, 2026); the compiled table used here was provided by the Jefferson Project at Lake George. Ice-in requires complete ice cover from the south end of

10

https://doi.org/10.5194/egusphere-2026-6116
Preprint. Discussion started: 5 November 2026
© Author(s) 2026. CC BY 4.0 License.

the lake to the north end; ice-out requires that ice has cleared sufficiently for a boat to pass between Prisoners Island and the Steel Pier, near the village of Lake George at the southern end of the lake.

For the Huntington Wildlife Forest lakes, observations come from the Adirondack Long-Term Ecological Monitoring Program lake ice survey record maintained by the Adirondack Ecological Center, State University of New York College of Environmental Science and Forestry (McNulty, 2022).

For the remaining lakes, dates were drawn from the compiled Northern Hemisphere lake-ice phenology record of Sharma et al. (2022), which extends the Global Lake and River Ice Phenology Database archived at the National Snow and Ice Data Center (Benson et al., 2000).

For Lake Placid, Schroon Lake and Upper Saranac Lake, observations come from the Lake Ice Observation Network operated by the Paul Smith's College Adirondack Watershed Institute, a citizen-science program in which observers report the state of a lake surface on a four-level scale from open water to complete ice cover and may additionally flag an observation as the first ice-in or ice-out of the season (Adirondack Watershed Institute, 2026b). These records are opportunistic rather than scheduled, so the interval between successive observations varies from a day to several months, and we use only observations carrying an explicit ice-in or ice-out flag. Because these three lakes were not used in model development or cross-validation, they are treated as an independent test rather than added to the validation set (Sect. 3.4).

We exclude from validation any observed period whose break-up date falls before 1 January, which cannot represent a spring break-up, and any period shorter than six days. The six-day floor is set by the observing system rather than by the lakes: a period shorter than the shortest revisit interval cannot in principle be resolved from the satellite time series. The floor lies below the shortest season in the record, so no complete observed season is removed. Corrections applied to the compiled records before use are described in Sect. S2. Where a lake and season carry more than one observed period, records are collapsed by taking the earliest ice-in and the latest ice-out. We refer to this convention as the envelope policy because it takes the outer bounds of all recorded periods in that season; taking the first recorded period instead would select brief early freezes shorter than the revisit interval over the long seasons that follow them.

https://doi.org/10.5194/egusphere-2026-6116
Preprint. Discussion started: 5 November 2026
© Author(s) 2026. CC BY 4.0 License.

2.5 Rationale for the method design

The three failure modes of threshold detection described in Sect. 1, namely consolidation lag at freeze-up, between-lake differences in the absolute backscatter of an ice cover, and wind roughening of open water, each motivate a specific element of the design that follows. Because the transition is gradual, we estimate a probability of ice for each scene rather than applying a crossing point, and decode the season as a whole rather than scene by scene. Because absolute levels are not comparable between lakes, predictors are expressed as departures from a per-lake open-water reference and are centered within relative orbit. Because a single scene cannot separate wind-roughened water from ice, we admit an independent constraint in the form of accumulated degree-days, which enter both the per-scene model and the transitions of the temporal model, so that an event cannot be placed at a time when the thermal forcing could not have produced it.

The remainder of this section describes the method itself. Predictors are computed for every acquisition (Sect. 2.6); a statistical model converts them into a per-scene probability of ice (Sect. 2.7); and a temporal model resolves the season's probability sequence into a single ice-covered interval, from which the event dates and their resolution bounds are extracted (Sect. 2.8). A fixed-threshold baseline used for comparison is described in Sect. 2.9, and the evaluation protocol in Sect. 2.10. The configuration was fixed before the model was applied to the validation lakes or to the production dataset, with no per-lake tuning. Fig. 2 summarizes the workflow.

12

https://doi.org/10.5194/egusphere-2026-6116
Preprint. Discussion started: 5 November 2026
© Author(s) 2026. CC BY 4.0 License.

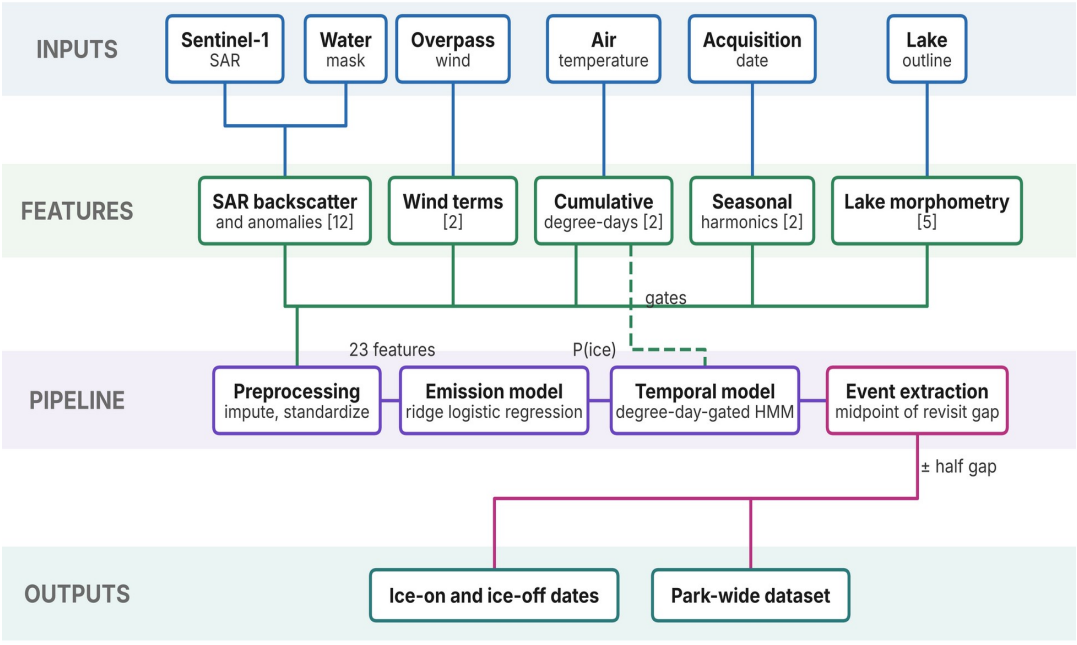


Figure 2. Workflow for deriving ice-on and ice-off dates from Sentinel-1 and reanalysis inputs. Numbers in brackets give the number of predictors in each group (Sect. 2.6, Table S4).

2.6 Predictors

Each acquisition is described by 23 predictors in five groups, listed with their definitions, units and sources in Table S4.

Backscatter statistics (seven predictors). We use the median and spatial standard deviation of VV and of VH over the lake's water pixels, the difference between median VV and median VH in decibels, the range between the 10th and 90th percentiles of VV, and the linear depolarization ratio VH/VV. The VV−VH difference is an exact linear combination of the two channel medians and therefore carries no information beyond them in a linear model; it is retained because it is the physically interpretable contrast between co- and cross-polarized return, and because the L2 penalty distributes weight across correlated predictors rather than selecting arbitrarily between them.

Open-water baseline anomalies (three predictors). Absolute backscatter over a lake depends on lake-specific properties that do not change through a season, including fetch, shoreline geometry and the mix of scattering surfaces within the water mask, so a fixed decibel threshold

13

https://doi.org/10.5194/egusphere-2026-6116
Preprint. Discussion started: 5 November 2026
© Author(s) 2026. CC BY 4.0 License.

applied across lakes performs poorly. For each lake and season we established an open-water reference level as the median of the acquisitions of October and November, a fixed calendar window that precedes freeze-up in nearly every lake-season of the record, and expressed the VV−VH difference, the VV median and the VV spatial standard deviation as departures from that reference. No observed ice date enters this step, so the reference carries no information from the validation records into the cross-validation.

Orbit-phase centering (two predictors). Sentinel-1 images a given lake from several relative orbits, each with its own incidence angle and look direction, and backscatter for an unchanged surface differs systematically between them. The VV−VH difference and the VV median were therefore also mean-centered within relative orbit, so that a departure is measured against acquisitions of the same lake in the same viewing geometry.

Wind predictors (two predictors). Wind roughens an open-water surface and raises its backscatter, which can mimic the brightening produced by ice cover (Sobiech and Dierking, 2013; Antonova et al., 2016). Two predictors let the model discount this: wind speed at the overpass, and a wind-decorrelation term measuring how strongly a lake's departures from the open-water reference co-vary with overpass wind speed across the acquisitions of a season,

$$\Delta_wd = corr(\ \sigma°_obs - \sigma°_ref\ ,\ U_overpass\ ) \quad (1)$$

where σ°_obs is the observed VV−VH contrast at each overpass, σ°_ref the open-water reference, U_overpass the concurrent wind speed, and the correlation is computed over all acquisitions of the lake-season, so that Δ_wd takes a single value for each lake and season. The difference σ°_obs − σ°_ref isolates excess surface brightness. Over ice this excess is high but largely uncoupled from wind; over rough open water it tracks wind speed closely, so a large Δ_wd identifies brightening as roughness-driven rather than ice-driven.

Thermodynamic, seasonal and morphometric predictors (nine predictors). Cumulative FDD and TDD; the sine and cosine of day-of-year, which express the seasonal cycle without imposing a break at the year boundary; and five static lake properties, namely surface area on a logarithmic scale, maximum depth, elevation, a fetch proxy, and a depth-known flag. The fetch proxy is the square root of surface area, a length scale standing in for the distance over which wind can act on the surface; it is an exact function of area and is included because that length scale, rather than

https://doi.org/10.5194/egusphere-2026-6116
Preprint. Discussion started: 5 November 2026
© Author(s) 2026. CC BY 4.0 License.

area itself, is the quantity relevant to wind-driven roughening. The depth-known flag indicates whether a measured depth exists for that lake, so that the model can distinguish a measurement from a substituted value.

Missing predictor values were replaced by the median of the corresponding predictor (no values were missing in the final production table), and all predictors were then rescaled to zero mean and unit variance so that fitted coefficients are comparable across predictors of different physical units.

2.7 Emission model

The per-scene probability of ice is estimated with ridge (L2-regularized) logistic regression, the standard form for a binary outcome (McCullagh and Nelder, 1989) with a penalty that stabilizes the fit when predictors are correlated (Hoerl and Kennard, 1970; Hastie et al., 2009), fitted on the 23 standardized predictors with the two classes weighted inversely to their frequency in the training set. The model returns a value between zero and one for each acquisition, interpreted as the probability that the lake was ice-covered at that time. For standardized predictor vector x_i at acquisition i,

$$P(ice \mid x_i) = \sigma(\beta_0 + \beta^T x_i) , \quad \sigma(z) = 1 / (1 + e^{-z}) \tag{2}$$

with coefficients estimated by minimizing the penalized negative log-likelihood,

$$\beta = \mathrm{argmin}_\beta \left[-\sum_i \left(y_i \ln p_i + (1 - y_i) \ln(1 - p_i) \right) + \lambda \|\beta\|_2^2 \right] \tag{3}$$

where p_i = P(ice | x_i) from Eq. (2), y_i ∈ {0, 1} is the training label and λ > 0 sets the penalty strength. The L2 penalty shrinks coefficients in proportion to their magnitude, stabilizing the fit when predictors are correlated, as the backscatter predictors necessarily are (Hoerl and Kennard, 1970; Hastie et al., 2009).

The model fuses radar and meteorological information rather than post-processing a radar model with meteorology. Cumulative degree-days, the seasonal harmonics and the static lake properties establish a prior expectation of ice at a given point in a season, and the backscatter predictors supply the observational correction that distinguishes one lake or season from another under similar thermal forcing.

2.8 Temporal model and event extraction

15

https://doi.org/10.5194/egusphere-2026-6116
Preprint. Discussion started: 5 November 2026
© Author(s) 2026. CC BY 4.0 License.

Individual scenes are noisy, and a lake does not alternate between frozen and open on the timescale of a single revisit. We therefore estimate the most likely state sequence for the season using a two-state hidden Markov model with hidden states s ∈ {water, ice}, solved by the Viterbi algorithm (Viterbi, 1967; Rabiner, 1989). The emission model supplies the emission term b_i(s), the probability of the observation at acquisition i under state s, and a transition matrix A(s′→s) encodes state persistence. The probability of a change of state between consecutive acquisitions is proportional to the length of the revisit gap, at 0.02 per day and capped at 0.45, so that persistence is expressed per unit time rather than per scene and a long gap does not suppress a transition that the observations support.

Transitions are additionally gated by a factor g_i(s′→s), equal to one if the transition is thermodynamically admissible at acquisition i and to 0.02 otherwise, which makes an inadmissible transition effectively unreachable while keeping the recursion numerically stable. Water-to-ice transitions were admitted only after cumulative freezing degree-days reached 20 °C·d, and ice-to-water transitions only after cumulative thawing degree-days reached 15 °C·d. These values were chosen from the training observations as conservative lower bounds: cumulative TDD at the first acquisition after an observed break-up is never below 30 °C·d, and cumulative FDD at the first acquisition after an observed freeze-up exceeds 20 °C·d in all but four of the 79 validation lake-seasons, with a minimum of 14 °C·d on three small lakes. The gates therefore exclude only thermodynamically implausible transitions rather than determining the event dates themselves. Both thresholds were fixed before cross-validation and prospective evaluation. Because they were chosen with all 13 validation lakes in view, Table S5 reports the sensitivity of the results to their values: freeze-up and break-up errors change by less than 1 d for freezing gates between 10 and 60 °C·d and thawing gates between 5 and 45 °C·d, and removing the gates altogether changes freeze-up error from 11.5 to 12.5 d and break-up error from 8.3 to 8.2 d, so the choice of gate values cannot have affected the score of any held-out lake. The degree-day predictors of the emission model and the gates play different roles: the former shift the per-scene probability continuously, whereas the gates only forbid transitions before a minimal accumulation and do not alter probabilities within the admissible range. The most probable state sequence follows from the gated recursion:

$$\delta_i(s) = b_i(s) \cdot \max_{s'} \left[\delta_{i-1}(s') \cdot A(s' \to s) \cdot g_i(s' \to s) \right], \quad \delta_1(s) = \pi(s)\, b_1(s) \tag{4}$$

16

https://doi.org/10.5194/egusphere-2026-6116
Preprint. Discussion started: 5 November 2026
© Author(s) 2026. CC BY 4.0 License.

where $\pi(s)$ is the initial state distribution, with the optimal path recovered by back-tracking. The thermodynamic gates prevent the temporal model from placing transitions that are inconsistent with the accumulated thermal forcing. Freeze-up requires sufficient prior heat loss, whereas break-up requires sufficient heat input; consequently, a freeze-up before meaningful cold accumulation or a break-up before meaningful warm accumulation is rejected regardless of the radar signal (Williams, 1965; Ashton, 1986; Leppäranta, 2023). Fig. 3 illustrates the complete processing chain for a representative lake, including the SAR observations, emission-model probabilities, and the decoded seasonal ice state.

The temporal model returns the acquisition at which the state changes, not the day on which the lake froze or cleared. The true transition occurred between the last acquisition in the previous state and the first acquisition in the new state. We call the interval between these two consecutive acquisitions the revisit gap, and report the event date as its midpoint with a resolution bound of plus or minus half the gap. Every event carries its own interval, and intervals differ between events because the sampling does. This interval is the sampling resolution of the estimate, not its total uncertainty: the cross-validated errors reported in Sect. 3.1, which include model error, are the expected accuracy of an individual event, and the half-gap is the floor set by the observing system below which no method can place an event.

17

https://doi.org/10.5194/egusphere-2026-6116
Preprint. Discussion started: 5 November 2026
© Author(s) 2026. CC BY 4.0 License.

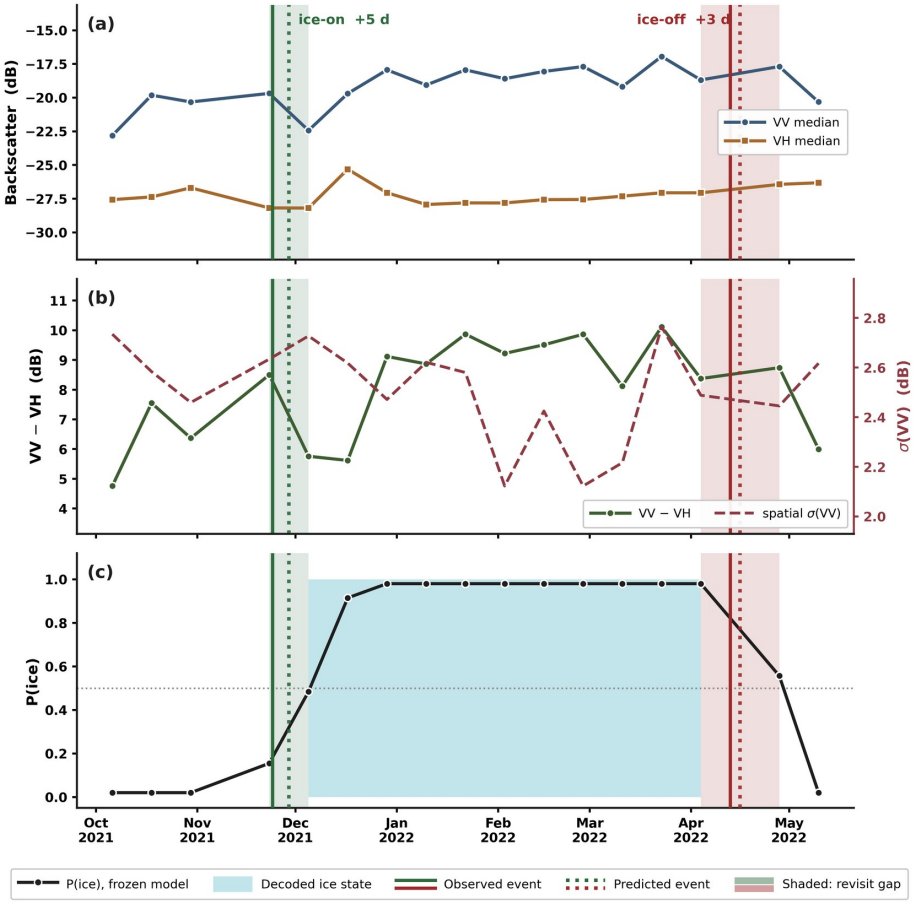


Figure 3. Worked example for Arbutus Lake, winter 2021–22. (a) Median VV and VH backscatter. (b) VV−VH difference and spatial standard deviation of VV. (c) Emission-model probability of ice and the decoded ice state, with observed (solid) and modelled (dotted) ice-on (green) and ice-off (red) dates.

2.9 Threshold baseline for comparison

To place the method in context we implemented a fixed-threshold detector representative of the class of approach described in Sect. 1, referred to here as Rule A, and applied it to the same lakes and seasons. The VV−VH difference is smoothed with a three-scene centered rolling median. An open-water reference is taken as the median of the first four smoothed values of the season, or of the first third of the season where fewer scenes are available, and the freeze level is set 3 dB above that reference, representing an approximately twofold increase in radar backscatter intensity on a logarithmic decibel scale (Ulaby et al., 1986). Freeze-up is declared at the first scene of the earliest four-scene window in which at least three values lie at or above the freeze

18

https://doi.org/10.5194/egusphere-2026-6116
Preprint. Discussion started: 5 November 2026
© Author(s) 2026. CC BY 4.0 License.

level and the first value of the window also does so. For break-up, the winter maximum is taken as the 90th percentile of smoothed values after freeze-up, and a break-up level is set 3 dB below it, and the same window rule is applied with the inequality reversed. Seasons with fewer than five acquisitions return no event, and in seasons with fewer than fifteen the window is shortened to two scenes with no tolerance. The 3 dB offset and the persistence rule are applied identically to every lake, and no parameter is fitted. Rule A is intended as a representative fixed-offset detector rather than as the best available threshold method; per-lake adaptive thresholds and unsupervised classification (Sobiech and Dierking, 2013; Murfitt and Duguay, 2020) can do better on individual lakes, and the comparison should be read as establishing what the fused model adds over a simple detector applied without local tuning.

2.10 Validation design

The model is scored by leave-one-lake-out cross-validation, a blocked design in which the unit held out is the lake rather than the scene (Roberts et al., 2017). For each of the 13 validation lakes in turn, the emission model is refitted on the remaining lakes and used to score the held-out lake, so no lake's own observations contribute to the model that scores it; within each fold the fill-in and standardization constants are computed from the training lakes only. This design targets the specific failure mode that matters for a method intended to be applied to unmonitored lakes. Because eight of the thirteen lakes form the Huntington cluster, we also report a leave-one-cluster-out variant in which all eight are held out together and the emission model is fitted on the five remaining lakes (Table S6).

For each detected event we report the signed difference from the observed date, together with the detection rate, meaning the fraction of lake-seasons in which an event was resolved at all. Detection rate and error are computed on the 79 lake-seasons that carry a complete observed ice period; the four documented no-freeze seasons are scored separately, as false positives when a model declares an ice event in them (Table 2, final column), and seasons with only an ice-in or only an ice-out observation are excluded. We also report the per-scene area under the receiver operating characteristic curve (AUC; Fawcett, 2006), which measures how well a model separates ice scenes from water scenes without reference to any particular probability cut-off: it equals the probability that a randomly chosen ice scene is assigned a higher P(ice) than a randomly chosen water scene, so that 0.5 indicates no skill and 1.0 perfect separation.

19

https://doi.org/10.5194/egusphere-2026-6116
Preprint. Discussion started: 5 November 2026
© Author(s) 2026. CC BY 4.0 License.

Classifying individual scenes correctly is not the same as dating the transition between states, because the date depends only on the few scenes that bracket the change, and a model can label almost every scene in a season correctly while still placing that change several revisit intervals away from the observed date; error in the event date and the fraction of seasons in which an event is resolved are therefore the quantities that matter for the intended use. Mean absolute error (MAE) is conditional on an event having been detected at all, so a model configuration that resolves few seasons is scored only on the seasons it resolves and cannot be compared on error alone with one that resolves most of them.

3 Results

3.1 Accuracy and error structure

Across the 79 validation lake-seasons the developed model resolves 73 freeze-up events and 70 break-up events. Against observed dates, freeze-up carries a mean absolute error of 11.5 d (RMSE 14.9 d, bias +4.0 d, r = 0.71) and break-up 8.3 d (RMSE 10.2 d, bias +1.6 d, r = 0.66). Both biases are positive, meaning predicted events fall slightly later than observed ones on average, but in both cases the bias is small relative to the scatter and to the 12-day sampling interval. Fig. 4 shows the full distribution.

Two features of the figure matter for interpretation. First, the resolution bars are not uniform: they span half the revisit gap bracketing each transition, so events resolved across a longer sampling gap are correspondingly less precise, and the widest bars carry the least information. Second, the shaded band marks one revisit interval either side of the 1:1 line, which is approximately the precision the observing system can deliver. Errors falling inside that band are not distinguishable from sampling resolution.

https://doi.org/10.5194/egusphere-2026-6116
Preprint. Discussion started: 5 November 2026
© Author(s) 2026. CC BY 4.0 License.

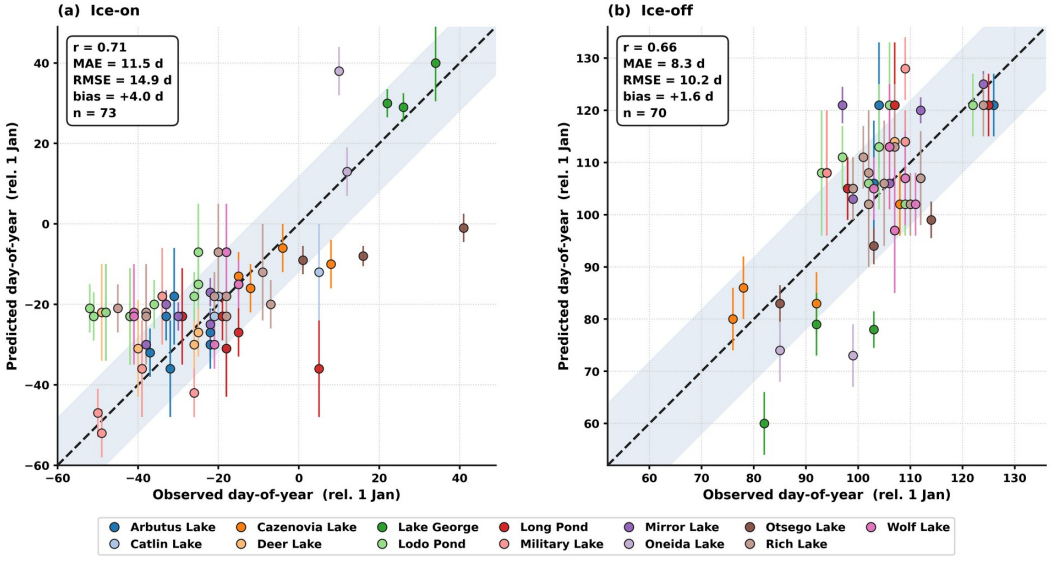


Figure 4. Predicted versus observed event dates under leave-one-lake-out cross-validation. (a) Freeze-up. (b) Break-up. Day-of-year is relative to 1 January of the season's end year. Bars span half the bracketing revisit gap, the sampling-resolution bound of each estimate.

Per-lake metrics are given in Table S3, but we report aggregates rather than a ranking: the envelope policy (Sect. 2.4) shifts error among the three lakes carrying multiple records for a season, leaving any ordering by accuracy unstable. Lake George (11,400 ha) and Oneida (20,670 ha), the two largest validation lakes, show both the largest break-up errors (20.0 and 18.5 d) and the lowest detection rates. Each is sampled as a single patch covering a small fraction of its surface (Sect. 2.2), which cannot resolve a spatially progressive break-up. Holding out the whole Huntington cluster at once (Table S6) leaves freeze-up on those eight lakes unchanged, at 11.5 d with every season detected, but raises their break-up error from 7.4 to 12.6 d and lowers break-up detection from 95 to 77 %.

3.2 Model comparison and the contribution of SAR

Table 2 compares the fused model against three reduced variants: a meteorology-only model that uses only the cumulative degree-days and the seasonal harmonics, a SAR-only model that uses only the backscatter and wind predictors, and Rule A, the fixed-threshold baseline of Sect. 2.9. The static morphometric predictors are withheld from both reduced models so that each isolates a single observational source. All four are evaluated on the same 79 lake-seasons under the same cross-validation protocol.

21

https://doi.org/10.5194/egusphere-2026-6116
Preprint. Discussion started: 5 November 2026
© Author(s) 2026. CC BY 4.0 License.

Model variant	AUC	Freeze-up detected	MAE (d)	Bias (d)	Break-up detected	MAE (d)	Bias (d)	No-freeze false positives
Meteorology-only	0.966	75/79 (95%)	16.1	+4.8	75/79 (95%)	8.2	−0.9	4/4
SAR-only	0.813	67/79 (85%)	17.0	+8.4	50/79 (63%)	14.5	−6.1	3/4
Fused (this study)	**0.993**	**73/79 (92%)**	**11.5**	**+4.0**	**70/79 (89%)**	**8.3**	**+1.6**	**1/4**
Rule A (baseline)	n/a	43/79 (54%)	36.1	+31.8	9/79 (11%)	23.4	−23.4	2/4

Table 2. Performance of the fused model developed here against three alternatives: a meteorology-only null, a SAR-only model, and the fixed-threshold baseline (Rule A). Evaluated on 79 validation lake-seasons from 13 lakes under leave-one-lake-out cross-validation. AUC is the receiver operating characteristic curve and MAE is Mean Absolute Error.

Detection rate and error must be read together. Rule A resolves break-up in 9 of 79 seasons, so its 23.4 d error is measured on the nine seasons it happens to resolve and is not comparable with variants resolving 70 or more. Its more consequential failure is coverage rather than accuracy: a method that returns no answer for 89% of break-up events cannot support a park-wide dataset. Rule A also yields no per-scene probability, so no AUC is defined for it.

Comparing the fused model with the meteorology-only model separates the two events clearly. For freeze-up, adding the SAR predictors reduces the mean absolute error from 16.1 d to 11.5 d, an improvement of 4.6 d (28 %); a paired bootstrap that resamples the 13 lakes with replacement gives a 95 % interval of −0.3 to 11.3 d for this improvement, with a probability of 0.035 that it is zero or negative, so with 13 lakes the evidence is suggestive rather than conclusive and the no-freeze test of Sect. 3.3 provides the independent support. For break-up, the error changes only from 8.2 d to 8.3 d, with a bootstrap interval of −2.4 to +1.7 d, indicating no measurable contribution from SAR. This asymmetry suggests that SAR provides additional information primarily during freeze-up.

Grouping the fitted standardized coefficients by summed absolute magnitude gives seasonal harmonics 29.1%, cumulative degree-days 26.7%, the twelve SAR predictors 25.1%, static morphometry 18.4% and wind 0.6%. The single largest coefficient is cumulative TDD, so meteorology enters the per-scene probability directly and not only through the temporal stage. These shares ignore correlation between predictors and should be read as indicative rather than as a variance decomposition.

22

https://doi.org/10.5194/egusphere-2026-6116
Preprint. Discussion started: 5 November 2026
© Author(s) 2026. CC BY 4.0 License.

The wind predictors carry 0.6% of the total absolute weight, the two smallest coefficients in the model. This is not an artifact of missing data: both are fully populated and retain their full range. Substituting median values for both altered the decoded event in 64 of 1,310 lake-seasons, or 4.9%, almost all by a single revisit interval, while changing break-up error by 0.19 d and freeze-up error not at all. We had expected these predictors to suppress wind-driven false positives on open water, and they do not measurably do so; that role is instead carried by the meteorological predictors and the thermodynamic gates.

Seven of the 79 validation lake-seasons carry more than one observed period, on Cazenovia, Mirror and Oneida. The envelope policy of Sect. 2.4 is adopted as primary; Table S7 shows that the alternative of taking the single longest recorded period leaves the fused model's freeze-up error unchanged and changes its break-up error by 0.5 d.

3.3 Discrimination of no-freeze seasons and the prospective test

The archive contains four documented seasons in which a validation lake did not freeze. All four are Lake George: 2017–18, 2019–20, 2022–23 and 2023–24. This is the sharpest available test of whether a model has learned the calendar rather than the lake, because in each of these seasons a calendar-driven model would declare ice and be wrong.

The meteorology-only model declares ice in all four, the SAR-only model in three and the fused model in one (Table 2, final column). Winter 2023–24 is the clearest case and is shown in Fig. 5c: the meteorology-only model peaks at P = 0.87 and decodes 12 ice scenes, the SAR-only model peaks at P = 0.95, and the fused model peaks at P = 0.54 and decodes none. Both single-source models fail on the same season that their combination resolves correctly. The fused model correctly rejected three of the four documented no-freeze winters.

The residual detection is 2017–18, shown in Fig. 5b. The fused model decodes ice in 8 of 53 scenes with a peak probability of 0.84, from about 22 January to 25 February 2018, following the cold wave of late December 2017 and early January 2018. Whether this is a model error or a definitional mismatch cannot be settled from the record alone: the sampled patch lies in the southern basin, whereas the Association's ice-in criterion requires complete cover from the south end of the lake to the north end, so ice that formed and persisted on the sampled patch without

https://doi.org/10.5194/egusphere-2026-6116
Preprint. Discussion started: 5 November 2026
© Author(s) 2026. CC BY 4.0 License.

the lake freezing over completely would register as ice in the SAR series and as no freeze in the record.

The Lake George Association declared ice-in on 26 January 2026 and ice-out on 2 April 2026. The cross-validated model estimated freeze-up on 29 January (3 days late) and break-up on 20 March (13 days early) (Fig. 5a). The production model, retrained using all available observations, estimated freeze-up on 28 January (2 days late) and break-up on 20 March, the same date as the cross-validated model. Both results are reported because the deposited production dataset and the cross-validated evaluation represent separate analysis products.

The freeze-up agreement is within a quarter of the revisit interval and within the model's typical error on this lake. The 13-day early break-up reflects the difference between melt onset, to which C-band backscatter responds, and the Association's navigability criterion; melt onset necessarily precedes navigability, so the break-up dates of this dataset should be read as melt onset and an offset expected against observer records.

https://doi.org/10.5194/egusphere-2026-6116
Preprint. Discussion started: 5 November 2026
© Author(s) 2026. CC BY 4.0 License.

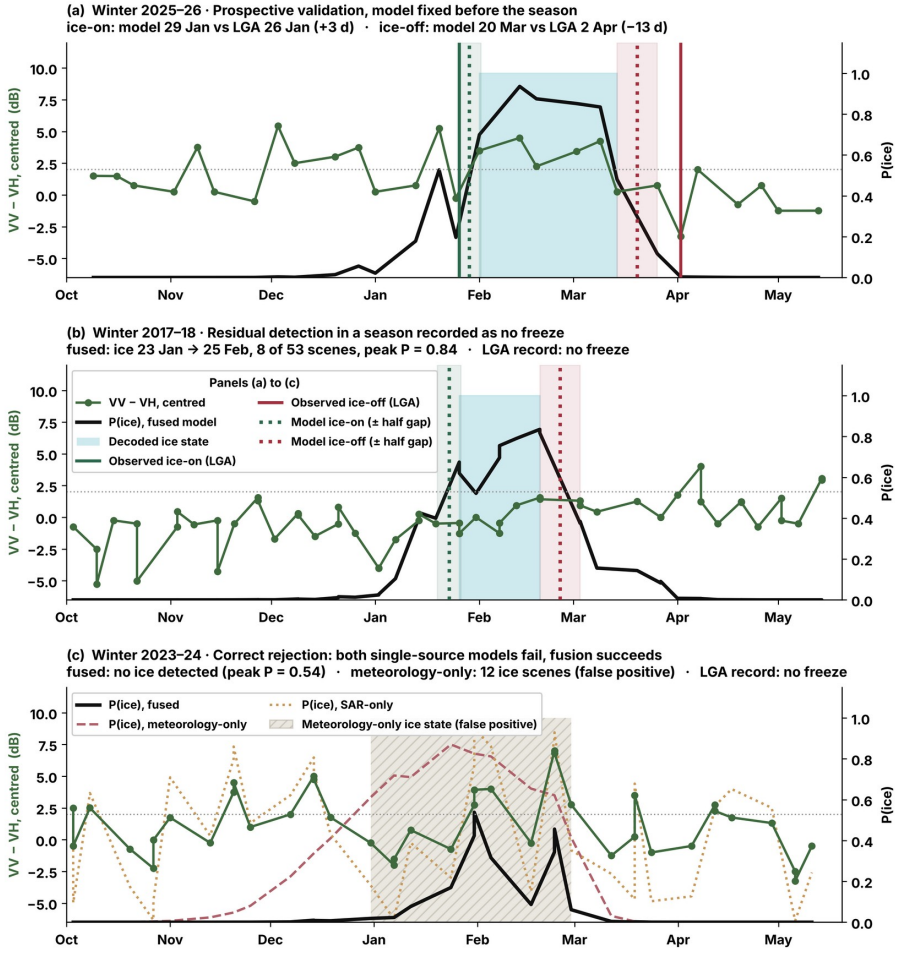


Figure 5. Lake George in (a) winter 2025–26, the prospective test, and in (b) winter 2017–18 and (c) winter 2023–24, both recorded as no-freeze winters. Green: orbit-centered VV−VH contrast (left axis); black: fused-model probability of ice (right axis); shading: decoded ice state. Solid vertical lines are observed events and dotted lines model estimates (green ice-on, red ice-off). Panel (c) also shows the meteorology-only and SAR-only probabilities.

3.4 Independent test on three previously unvalidated lakes

Observations from the Lake Ice Observation Network provide five flagged events on three lakes that were used neither in model development nor in cross-validation: one freeze-up and one break-up on Upper Saranac Lake, and one break-up each on Lake Placid, Schroon Lake and Upper Saranac Lake in 2022–23. Because these lakes belong to the application set, predictions for them already existed in the production dataset and were not recomputed. Table 3 compares them with the observed dates.

25

https://doi.org/10.5194/egusphere-2026-6116
Preprint. Discussion started: 5 November 2026
© Author(s) 2026. CC BY 4.0 License.

Lake	Season	Event	Observed	Predicted	Error (d)	Resolution bound (±d)	Scenes	QC flag
Lake Placid	2022–23	Break-up	13 Apr 2023	14 Apr 2023	+1	3.5	21	—
Schroon Lake	2022–23	Break-up	12 Apr 2023	2 Apr 2023	−10	8.5	28	—
Upper Saranac Lake	2022–23	Break-up	14 Apr 2023	23 Apr 2023	+9	12.0	11	sparse sampling
Upper Saranac Lake	2023–24	Freeze-up	23 Dec 2023	19 Dec 2023	−4	12.0	9	sparse sampling
Upper Saranac Lake	2023–24	Break-up	19 Mar 2024	17 Apr 2024	+29	12.0	9	sparse sampling

Table 3. Independent test on three lakes not used in model development or cross-validation, against observations from the Lake Ice Observation Network.

Three of the five predictions fall within their stated resolution bound. Mean absolute error across all five is 10.6 d, against 8.3 d for break-up and 11.5 d for freeze-up in the cross-validated set. The single largest error, 29 d on the Upper Saranac break-up of 2023–24, occurs in a season that the production pipeline had already flagged for sparse scene coverage, with nine acquisitions and a stated resolution bound of ±12 d. Excluding that season, mean absolute error across the remaining break-up events is 6.7 d with no bias.

The sample is too small to establish a meaningful difference in either direction. Resampling four break-up events from the cross-validated error distribution yielded a median mean absolute error of 7.8 d and a 90 % interval of 3.8-13.5 d. The observed mean absolute error of 12.2 d for the four new break-up events falls at the 90th percentile of this distribution, while the value decreases to 6.7 d (38th percentile) after excluding the flagged season. Both values are therefore consistent with the variability expected from the cross-validated error distribution.

Two differences from the other ground-truth sources should be noted. The Observation Network records complete clearance of ice rather than the navigability criterion applied on Lake George, and three of the five events have no preceding observation within the same season, so the observed dates themselves carry uncertainty that the scheduled records do not.

3.5 Park-wide ice phenology, 2016 to 2026

26

https://doi.org/10.5194/egusphere-2026-6116
Preprint. Discussion started: 5 November 2026
© Author(s) 2026. CC BY 4.0 License.

Applying the developed model to all 131 lakes across the ten winters yields 1,310 lake-season records. Events were resolved for every lake-season in every area class below 1,000 ha. The exception is Lake George, where events were resolved in five of ten winters, four of the remaining five being the documented no-freeze seasons discussed above.

Records carry quality-control flags recording the conditions under which they were produced (Table 4). Of the 1,310 records, 110, or 8.4%, carry at least one flag. None are excluded. A flag marks a record as produced under conditions where the method is known to be weaker, most often sparse scene coverage.

Quality-control flag	Records	% of dataset	Action
None	1,200	91.6	Not flagged
Sparse sampling	90	6.9	Retained
Low elevation, long fetch	10	0.8	Retained
Large-lake melt onset	9	0.7	Retained
Melt onset and partial ice	1	0.1	Retained
Total flagged	**110**	**8.4**	**None excluded**

Table 4. Origin of quality-control flags across the 1,310 lake-season records of the park-wide dataset.

Mean ice duration falls monotonically with lake size across the area classes, from 149 d for the two lakes below 10 ha to 118 d for the 110 lakes between 50 and 200 ha, 113 d for the 16 lakes between 200 and 1,000 ha, and 43 d for Lake George. The park-wide median is approximately 120 d.

Between-winter variability is large and tracks the thermal forcing closely (Fig. 6). The longest median durations occur in 2017–18 and 2018–19, at 132 d and 129 d, and the shortest in 2023–24, at 96 d: a swing of 36 days, or about a fifth of the ice season, between the coldest and warmest winters in a ten-year record. Across the ten winters of the study period, median duration and season-total freezing degree-days are correlated at $r = +0.72$ ($p = 0.019$, 95 % confidence interval 0.17 to 0.93, $n = 10$ winters; Spearman $\rho = 0.66$, $p = 0.04$). The interquartile range is zero in some seasons, which reflects the quantization imposed by a 12-day revisit rather than genuine agreement between lakes.

https://doi.org/10.5194/egusphere-2026-6116
Preprint. Discussion started: 5 November 2026
© Author(s) 2026. CC BY 4.0 License.

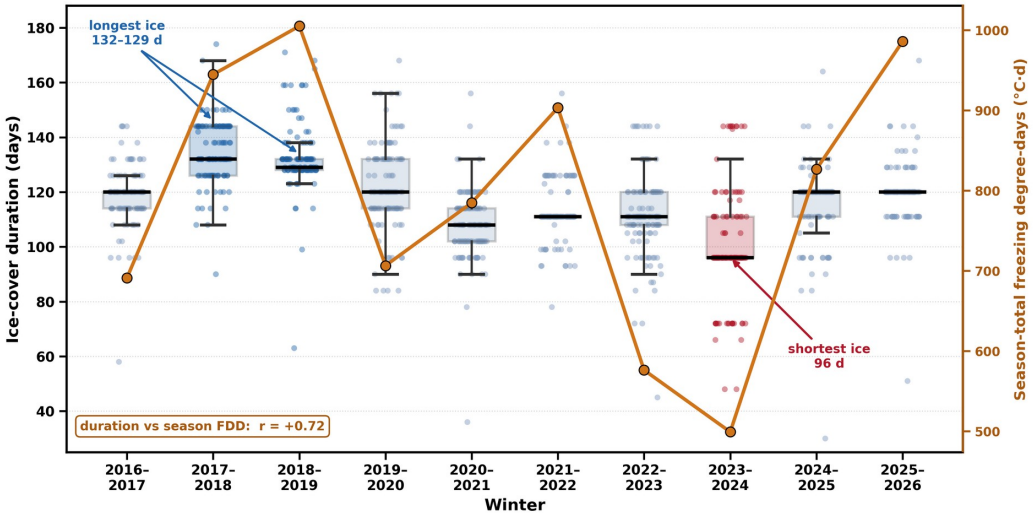


Figure 6. Ice-cover duration across 131 lakes for each of ten winters, with season-total freezing degree-days overlaid. Each point is one lake; boxes span the interquartile range, the horizontal line within each box marks the median, and whiskers indicate the extent of the remaining values.

Across lakes, elevation is the dominant control on mean duration (Fig. 7a). Ordinary least squares gives an increase of 6.0 d per 100 m of elevation, with r = 0.66 and $p < 0.001$ across the 131 lakes, and a robust Theil–Sen estimator gives 4.3 d per 100 m. The gradient is consistent with the lapse-rate control on accumulated freezing degree-days: across the same lakes, season-total FDD increases by 89 °C·d per 100 m of elevation (r = 0.97) and mean duration increases by 0.067 d per °C·d, which together imply 5.9 d per 100 m. Surface area is also negatively related to duration (Fig. 7b), but the gradient is sensitive to how it is estimated: ordinary least squares over all lakes gives −22 d per order of magnitude in area with r = −0.58, excluding Lake George gives −16 d with r = −0.40, and a robust Theil–Sen estimator gives −12 d. Elevation and log area are only weakly correlated in this set (r = −0.24), and a joint regression of mean duration on both gives 5.1 d per 100 m (95 % confidence interval 4.0 to 6.0) and −17 d per order of magnitude in area (−21 to −13), with $R^2 = 0.63$; excluding Lake George gives 4.9 and −12, and a robust Huber fit 4.5 and −13. Lake George and South Bay are high-leverage points in the area relationship. We therefore have more confidence in the elevation relationship, whose slope changes by about a quarter between estimators, than in the area effect, whose slope changes by nearly half. Lake area may well exert a strong control on duration, consistent with empirical models in which ice

28

https://doi.org/10.5194/egusphere-2026-6116
Preprint. Discussion started: 5 November 2026
© Author(s) 2026. CC BY 4.0 License.

phenology responds to both air temperature and lake morphometry (Shuter et al., 2013), but the present sample contains too few very small and very large lakes to constrain its magnitude.

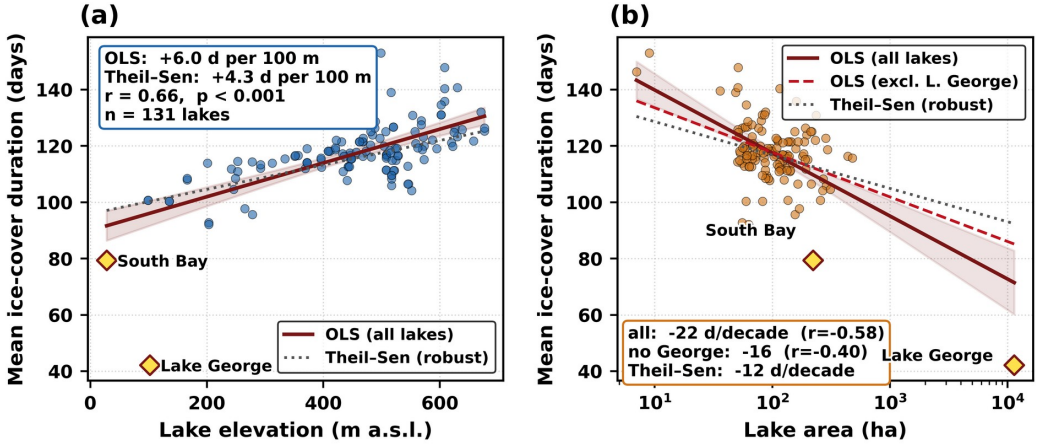


Figure 7. Controls on mean ice-cover duration across 131 lakes. (a) Elevation, with ordinary least squares and Theil–Sen fits. (b) Surface area on a logarithmic axis, with three fits: ordinary least squares over all lakes, the same excluding Lake George, and a Theil–Sen estimator. Lake George and South Bay are marked as high-leverage points in both panels.

4 Discussion

The contrasting contributions of SAR to freeze-up and break-up are consistent with the different physical controls governing the two transitions. Break-up is largely determined by cumulative heat input, so accumulated thawing degree-days already provide a strong predictor of event timing. Freeze-up is also thermodynamically constrained, by the heat stored in the water column, but that constraint depends largely on depth and mixing state, and depth is unmeasured for 123 of the 131 lakes. Whether a lake consolidates during a given cold period therefore depends on lake-specific factors such as thermal inertia, mixing state, wind exposure, and the persistence of newly formed ice, which the available meteorological and morphometric predictors represent only partially but which are directly reflected in SAR observations of the lake surface. Part of the radar's contribution at freeze-up may thus be compensation for missing heat-storage information. Fuller depth coverage, from the Adirondack Lakes Survey, from bathymetric surveys held by the Adirondack Watershed Institute and the New York State Department of Environmental Conservation, or from the regional Northeast Lake and Pond Classification, is the most promising route to improving the thermodynamic prior and is left to future work. The two

29

https://doi.org/10.5194/egusphere-2026-6116
Preprint. Discussion started: 5 November 2026
© Author(s) 2026. CC BY 4.0 License.

transitions are therefore not mirror images of each other: break-up is governed largely by the heat budget of the atmosphere, which gridded temperature captures, whereas freeze-up is governed by the heat budget of the lake, which it does not, so the two require different sources of information and the radar adds substantial information at freeze-up and little at break-up.

This asymmetry is consistent with the longest local observer record. Across more than three decades at the Huntington Wildlife Forest, Beier et al. (2012) reported declines in ice-cover duration of up to 21 d per lake, driven mainly by later freeze-up and only partly by earlier break-up: November and December temperature and snow depth consistently predicted ice-in, and warming and declining snow in those months were consistent with later ice formation, whereas the absence of trends in March and April snow depth produced much weaker trends in ice-out. That record ends in 2007; the winters since have shown high variability between seasons of normal ice cover and seasons in which ice does not form until late December or January. The freeze-up transition is therefore both the event carrying the stronger climate signal in this region and the event at which the radar adds most to a thermodynamic prior.

A sampling consideration bears on break-up specifically. On lakes observed at near-daily SAR revisit, break-up has been reported as a two-stage signature: an initial drop in backscatter at melt onset, followed by a recovery as the wet surface drains and roughens during the melt period, and a second, final drop at ice loss (Murfitt and Duguay, 2020), a sequence that radiative-transfer modeling of C-band backscatter through the melt reproduces (Murfitt et al., 2024). At the 12-day Sentinel-1 revisit used here, a temperate melt period may be shorter than the interval between successive acquisitions, so that in some seasons the first acquisition after the onset captures the initial drop and in others it captures the final drop. This alone would introduce a spread of the order of the revisit interval into the break-up estimate, and it offers a physical reason why adding backscatter to accumulated thawing degree-days does not improve break-up in Sect. 3.2: the radar cannot resolve which stage of the melt it is seeing. Denser SAR revisit is the direct remedy; combining ascending and descending passes would halve the sampling interval at the cost of mixing two times of day and two viewing geometries, which the orbit-phase centering of Sect. 2.6 is designed to absorb.

The two largest validation lakes produced the largest break-up errors and the lowest detection rates. Both are represented by a single sampling patch covering only a small fraction of the lake

30

https://doi.org/10.5194/egusphere-2026-6116
Preprint. Discussion started: 5 November 2026
© Author(s) 2026. CC BY 4.0 License.

surface, whereas break-up on lakes of this size progresses spatially, with shallow and exposed areas clearing before deeper basins. Multi-basin sampling would likely better capture this spatial progression, but the available sample of only three lakes larger than 1,000 ha is insufficient to determine whether such an approach would improve performance. Within-lake spatial heterogeneity is a research question in its own right: decoding several patches per lake, or mapping the ice state at the pixel level, would turn a single event date into a spatial progression of freeze-up and break-up, and the present dataset provides the patch-level baseline against which such an extension can be tested.

The rejection of three of four no-freeze winters provides the strongest evidence that the model is not simply encoding seasonal timing. A model driven primarily by meteorology would predict ice formation in every sufficiently cold winter, as the meteorology-only model does here. The limitation is that all four no-freeze seasons come from a single lake, so the test demonstrates the underlying mechanism rather than providing a robust estimate of specificity. A well-powered assessment would require documented no-freeze winters from multiple lakes, which are not yet available. The wind predictors play no measurable part in this rejection (Sect. 3.2); it is explained by the meteorological predictors and the thermodynamic gating. Identifying such winters matters ecologically as well as statistically: a winter without ice cover has no inverse stratification, remains exposed to wind mixing and light throughout, and loses the under-ice phase of the seasonal cycle, with consequences for oxygen, thermal structure and the timing of spring mixing (Hampton et al., 2017; Sharma et al., 2019), so a method that can recognize ice-free winters at unmonitored lakes extends to those lakes a quantity that observer records provide for only a few.

Several assumptions bound where the method applies. It assumes an ice cover that forms and clears once, since the temporal model returns a single interval per season and would report the outer envelope of a season containing a mid-winter thaw. It assumes a lake large enough to retain usable water pixels after shoreline masking, untested below about 7 ha. It assumes usable ascending-node coverage, since the 12-day revisit sets the achievable precision; a posterior distribution over transition dates from the forward–backward algorithm, in place of the single most probable path used here, would turn the resolution bound into a full probability distribution for each event and is a natural extension. The validation evidence is also narrower than a count

https://doi.org/10.5194/egusphere-2026-6116
Preprint. Discussion started: 5 November 2026
© Author(s) 2026. CC BY 4.0 License.

of 13 lakes suggests, since eight of the ten in-park lakes lie in one cluster under a single observer protocol, leaving three broadly independent in-park locations, although the Huntington lakes do span 7 to 217 ha and some range of elevation and exposure. The leave-one-cluster-out test (Table S6) shows what this means for transfer: with no Huntington lake in training, freeze-up on those lakes is resolved as well as before, but break-up error rises from 7.4 to 12.6 d and break-up detection falls from 95 to 77 %, because the five remaining training lakes are dominated by three very large lakes whose break-up behaves differently. Break-up timing therefore transfers best between lakes of similar size, and application to lakes unlike any in the validation set should be read with that in mind. Application to the 121 lakes without ground truth rests on the recovery of physically expected gradients rather than on direct validation.

The accuracies obtained here can be placed against published satellite phenology. With daily MODIS observations over 296 Maine lakes of 0.13 to 305 km², Zhang and Pavelsky (2019) obtained mean absolute errors of 7.3 d for freeze-up and 5.5 d for break-up against observer records; with near-daily Sentinel-1 coverage of Lake Hazen, Murfitt and Duguay (2020) reported mean errors of 2 to 10 d for threshold and first-difference methods against visual interpretation of the imagery. Our 11.5 and 8.3 d at a 12-day revisit, with a resolution floor of ±6 d, sit within the same range once the sampling interval is accounted for, which indicates that revisit frequency rather than the retrieval is now the binding constraint. Machine-learning classifiers for SAR and optical imagery (Hoekstra et al., 2020; Tom et al., 2020; Wu et al., 2021) report per-pixel or per-scene classification accuracy, which, as noted in Sect. 2.10, is not the same quantity as event-date accuracy and cannot be compared directly.

Those gradients are the main evidence that the method behaves sensibly where no observations exist. Ten winters is too short to estimate a trend and we make none, but the between-winter signal is large, with a 36-day difference in median duration between the coldest and warmest winters, tracking season-total freezing degree-days. The elevation gradient of 6.0 d per 100 m is recovered across lakes never used to fit or tune the model. It also carries an ecological implication: as winters warm, the higher lakes of the park are likely to retain a seasonal ice cover longest, while low-elevation lakes approach intermittent cover first, as Lake George at about 100 m, with four ice-free winters in ten, already shows. Given the regional warming set out in Sect. 1 and the absence of observer records at any of the 121 application-only lakes, the value of the

https://doi.org/10.5194/egusphere-2026-6116
Preprint. Discussion started: 5 November 2026
© Author(s) 2026. CC BY 4.0 License.

dataset is as a consistent baseline against which future seasons can be compared. Because ice-cover duration governs light and gas exchange, winter oxygen, the timing of spring mixing and the under-ice phase of production (Sect. 1), such a regional record is also the first requirement for linking those ecosystem responses to winter conditions across lakes that have never been monitored.

Users interested in trend detection should read the reported errors against that purpose. Long observer records show freeze-up moving later by 5.8 d and break-up earlier by 6.5 d per 100 years across the Northern Hemisphere (Magnuson et al., 2000), about 0.6 d per decade, with faster recent rates of 1.5 to 2.2 d per decade in small north-temperate lakes (Hewitt et al., 2018) and declines in ice duration of up to 21 d over three decades at the Huntington Wildlife Forest (Beier et al., 2012). Freeze-up and break-up errors of 8 to 12 d are therefore one to two orders of magnitude larger than the decadal change they would be asked to detect, so a trend estimated from the method alone would need many decades to emerge from noise. The method is better suited to establishing a consistent multi-lake baseline against which future change can be measured than to estimating a trend from its own record, and its precision will improve with revisit frequency rather than with further modeling. More frequent public SAR observations, including the restored two-satellite Sentinel-1 constellation and planned L-band missions, would tighten the revisit-gap bound directly; commercial SAR at daily revisit would do so further at a cost.

5 Conclusions

Freeze-up and break-up dates can be recovered for lakes that have never been observed by combining Sentinel-1 backscatter with reanalysis thermodynamics in a single probabilistic model, without tuning any parameter to an individual lake. Under leave-one-lake-out cross-validation the method resolves freeze-up to 11.5 d and break-up to 8.3 d across 13 lakes spanning three orders of magnitude in surface area, and resolves both events in around 90 % of lake-seasons, where a fixed-threshold baseline of the kind most often applied to this problem returns no break-up date at all in the great majority of seasons.

The contribution of the radar is not uniform across the ice season, and this is the result we regard as most transferable to other work. Freeze-up and break-up are not mirror processes. Break-up is

33

https://doi.org/10.5194/egusphere-2026-6116
Preprint. Discussion started: 5 November 2026
© Author(s) 2026. CC BY 4.0 License.

well constrained by accumulated thawing degree-days alone, and adding backscatter does not improve it. Freeze-up is less well constrained by meteorology alone, because whether a lake consolidates during a given cold spell depends on stored heat, mixing and exposure that the available predictors represent only partly, and there the radar reduces error by 4.6 d. The combination also rejects no-freeze winters that neither source rejects alone.

Applied to 131 lakes over ten winters, the developed method yields 1,310 lake-season records with a resolution bound attached to every event. The resulting dataset provides a consistent baseline for a lake population in which observations are available for only a small fraction of lakes, together with evidence that the method behaves sensibly where no ground truth exists. The results indicate an elevation gradient of 6.0 d per 100 m and a correlation of r = +0.72 between freezing degree-days and median ice duration across the ten winters. Because it requires no local observations and no per-lake tuning, the method extends to the remaining lakes of the park and to comparable temperate lake districts wherever Sentinel-1 coverage and gridded temperature data are available.

Code and data availability

The developed model, the analysis notebook, the park-wide production dataset of 1,310 lake-season records and the corrected ground-truth compilation are archived at Zenodo (https://doi.org/10.5281/zenodo.23142788; Azarderakhsh et al., 2026). Sentinel-1 GRD data are freely available from the Copernicus Data Space Ecosystem (https://dataspace.copernicus.eu), Daymet Version 4 from the ORNL DAAC (https://doi.org/10.3334/ORNLDAAC/1840), ERA5-Land from the Copernicus Climate Data Store (https://cds.climate.copernicus.eu), and the Global Surface Water dataset from the European Commission Joint Research Centre (https://global-surface-water.appspot.com).

Author contributions

MA: conceptualization, formal analysis, validation, writing (original draft). SET: conceptualization, data curation, review of the manuscript. MM: conceptualization, data curation, review of the manuscript. SAM: data curation, review of the manuscript. MJG: data curation, review of the manuscript. BW: data curation. PBM: review of the manuscript. KCR: supervision, review of the manuscript.

https://doi.org/10.5194/egusphere-2026-6116
Preprint. Discussion started: 5 November 2026
© Author(s) 2026. CC BY 4.0 License.

Competing interests

The authors declare that they have no competing interests.

Acknowledgements

We thank the observers whose records made this evaluation possible, and the Lake George Association, the Darrin Fresh Water Institute and the Warren County Department of Public Works for maintaining and publishing the Lake George record; the compiled Lake George series was provided by the Jefferson Project at Lake George. Data sets were provided by the Adirondack Ecological Center, State University of New York College of Environmental Science and Forestry (ROR: https://ror.org/02g8zgp32). We also thank the Paul Smith's College Adirondack Watershed Institute for access to Lake Ice Observation Network records.

Generative AI tools were used in the preparation of this manuscript in two ways: for language editing and grammatical revision of author-written text, and to produce the schematic layout of Fig. 2. All scientific content, analysis, results and interpretation are the authors' own, and the authors take full responsibility for the content of the manuscript.

Financial support

This research was supported by the New York State Department of Environmental Conservation (NYSDEC) through its funding of the SCALE project.

References

Adirondack Lakes Survey Corporation: Adirondack Lakes Survey 1984–1987: an evaluation of fish communities and water chemistry, Adirondack Lakes Survey Corporation, Ray Brook, New York, 1990.

Adirondack Watershed Institute: Adirondack Lake Assessment Program, Paul Smith's College Adirondack Watershed Institute, Paul Smiths, New York, https://www.adkwatershed.org/adirondack-lake-assessment-program, last access: 19 September 2026, 2026a.

35

https://doi.org/10.5194/egusphere-2026-6116
Preprint. Discussion started: 5 November 2026
© Author(s) 2026. CC BY 4.0 License.



Adirondack Watershed Institute: Lake Ice Observation Network, Paul Smith's College Adirondack Watershed Institute, Paul Smiths, New York, https://www.adkwatershed.org/lake-ice-observation-network, 2026b.

Antonova, S., Duguay, C. R., Kääb, A., Heim, B., Langer, M., Westermann, S., and Boike, J.: Monitoring bedfast ice and ice phenology in lakes of the Lena River Delta using TerraSAR-X backscatter and coherence time series, Remote Sens., 8, 903, https://doi.org/10.3390/rs8110903, 2016.

Ashton, G. D.: River and Lake Ice Engineering, Water Resources Publications, Littleton, Colorado, 1986.

Atwood, D. K., Gunn, G. E., Roussi, C., Wu, J., Duguay, C., and Sarabandi, K.: Microwave backscatter from Arctic lake ice and polarimetric implications, IEEE Trans. Geosci. Remote Sens., 53, 5972–5982, https://doi.org/10.1109/TGRS.2015.2429917, 2015.

Azarderakhsh, M., Mossel, C., Bah, A. R., Malik, A., Khanom, F., Borrelli, J., McIntyre, P., Norouzi, H., and Rose, K.: Validation and trend analysis of satellite-derived surface water temperature observations over Adirondack lakes, Environ. Adv., 21, 100662, https://doi.org/10.1016/j.envadv.2025.100662, 2025.

Azarderakhsh, M., Tuttle, S. E., Munsi, M., McNulty, S. A., Glennon, M. J., Wiltse, B., McIntyre, P. B., and Rose, K. C.: All-weather lake-ice phenology from Sentinel-1 and reanalysis thermodynamics: model, code and 2016–2026 dataset for 131 Adirondack lakes, Zenodo [data set and code], https://doi.org/10.5281/zenodo.23142788, 2026.

Beier, C. M., Stella, J. C., Dovčiak, M., and McNulty, S. A.: Local climatic drivers of changes in phenology at a boreal-temperate ecotone in eastern North America, Climatic Change, 115, 399–417, 2012.

Benson, B., Magnuson, J., and Sharma, S.: Global Lake and River Ice Phenology Database, Version 1, National Snow and Ice Data Center, Boulder, Colorado, https://doi.org/10.7265/N5W66HP8, 2000 (updated 2020).

Brown, L. C. and Duguay, C. R.: The response and role of ice cover in lake-climate interactions, Prog. Phys. Geogr., 34, 671–704, 2010.

https://doi.org/10.5194/egusphere-2026-6116
Preprint. Discussion started: 5 November 2026
© Author(s) 2026. CC BY 4.0 License.



Carrea, L., Crétaux, J.-F., Liu, X., Wu, Y., Calmettes, B., Duguay, C. R., Merchant, C. J., Selmes, N., Simis, S. G. H., Warren, M., Yesou, H., Müller, D., Jiang, D., Embury, O., Bergé-Nguyen, M., and Albergel, C.: Satellite-derived multivariate world-wide lake physical variable timeseries for climate studies, Sci. Data, 10, 30, https://doi.org/10.1038/s41597-022-01889-z, 2023.

Duguay, C. R., Pultz, T. J., Lafleur, P. M., and Drai, D.: RADARSAT backscatter characteristics of ice growing on shallow sub-Arctic lakes, Churchill, Manitoba, Canada, Hydrol. Process., 16, 1631–1644, https://doi.org/10.1002/hyp.1026, 2002.

Duguay, C. R., Prowse, T. D., Bonsal, B. R., Brown, R. D., Lacroix, M. P., and Ménard, P.: Recent trends in Canadian lake ice cover, Hydrol. Process., 20, 781–801, https://doi.org/10.1002/hyp.6131, 2006.

Farr, T. G., Rosen, P. A., Caro, E., Crippen, R., Duren, R., Hensley, S., Kobrick, M., Paller, M., Rodriguez, E., Roth, L., Seal, D., Shaffer, S., Shimada, J., Umland, J., Werner, M., Oskin, M., Burbank, D., and Alsdorf, D.: The Shuttle Radar Topography Mission, Rev. Geophys., 45, RG2004, https://doi.org/10.1029/2005RG000183, 2007.

Fawcett, T.: An introduction to ROC analysis, Pattern Recogn. Lett., 27, 861–874, https://doi.org/10.1016/j.patrec.2005.10.010, 2006.

Gorelick, N., Hancher, M., Dixon, M., Ilyushchenko, S., Thau, D., and Moore, R.: Google Earth Engine: planetary-scale geospatial analysis for everyone, Remote Sens. Environ., 202, 18–27, https://doi.org/10.1016/j.rse.2017.06.031, 2017.

Gunn, G. E., Duguay, C. R., Atwood, D. K., King, J., and Toose, P.: Observing scattering mechanisms of bubbled freshwater lake ice using polarimetric RADARSAT-2 (C-band) and UW-Scat (X- and Ku-bands), IEEE Trans. Geosci. Remote Sens., 56, 2887–2903, https://doi.org/10.1109/TGRS.2017.2786158, 2018.

Hampton, S. E., Galloway, A. W. E., Powers, S. M., Ozersky, T., Woo, K. H., Batt, R. D., Labou, S. G., O'Reilly, C. M., Sharma, S., Lottig, N. R., Stanley, E. H., North, R. L., Stockwell, J. D., Adrian, R., Weyhenmeyer, G. A., Arvola, L., Baulch, H. M., Bertani, I., Bowman, L. L., Carey, C. C., Catalan, J., Colom-Montero, W., Domine, L. M., Felip, M., Granados, I., Gries, C.,

https://doi.org/10.5194/egusphere-2026-6116
Preprint. Discussion started: 5 November 2026
© Author(s) 2026. CC BY 4.0 License.



910 Grossart, H.-P., Haberman, J., Haldna, M., Hayden, B., Higgins, S. N., Jolley, J. C., Kahilainen,
911 K. K., Kaup, E., Kehoe, M. J., MacIntyre, S., Mackay, A. W., Mariash, H. L., McKay, R. M.,
912 Nixdorf, B., Nõges, P., Nõges, T., Palmer, M., Pierson, D. C., Post, D. M., Pruett, M. J., Rautio,
913 M., Read, J. S., Roberts, S. L., Rücker, J., Sadro, S., Silow, E. A., Smith, D. E., Sterner, R. W.,
914 Swann, G. E. A., Timofeyev, M. A., Toro, M., Twiss, M. R., Vogt, R. J., Watson, S. B.,
915 Whiteford, E. J., and Xenopoulos, M. A.: Ecology under lake ice, Ecol. Lett., 20, 98–111,
916 https://doi.org/10.1111/ele.12699, 2017.

917 Hastie, T., Tibshirani, R., and Friedman, J.: The Elements of Statistical Learning: Data Mining,
918 Inference, and Prediction, 2nd edn., Springer, New York, https://doi.org/10.1007/978-0-387-
919 84858-7, 2009.

920 Hewitt, B. A., Lopez, L. S., Gaibisels, K. M., Murdoch, A., Higgins, S. N., Magnuson, J. J.,
921 Paterson, A. M., Rusak, J. A., Yao, H., and Sharma, S.: Historical trends, drivers, and future
922 projections of ice phenology in small north temperate lakes in the Laurentian Great Lakes region,
923 Water, 10, 70, https://doi.org/10.3390/w10010070, 2018.

924 Hodgkins, G. A., James, I. C., and Huntington, T. G.: Historical changes in lake ice-out dates as
925 indicators of climate change in New England, 1850–2000, Int. J. Climatol., 22, 1819–1827,
926 2002.

927 Hoekstra, M., Jiang, M., Clausi, D. A., and Duguay, C.: Lake ice-water classification of
928 RADARSAT-2 images by integrating IRGS segmentation with pixel-based random forest
929 labeling, Remote Sens., 12, 1425, https://doi.org/10.3390/rs12091425, 2020.

930 Hoerl, A. E. and Kennard, R. W.: Ridge regression: biased estimation for nonorthogonal
931 problems, Technometrics, 12, 55–67, https://doi.org/10.1080/00401706.1970.10488634, 1970.

932 Kirillin, G., Leppäranta, M., Terzhevik, A., Granin, N., Bernhardt, J., Engelhardt, C., Efremova,
933 T., Golosov, S., Palshin, N., Sherstyankin, P., Zdorovennova, G., and Zdorovennov, R.: Physics
934 of seasonally ice-covered lakes: a review, Aquat. Sci., 74, 659–682,
935 https://doi.org/10.1007/s00027-012-0279-y, 2012.

https://doi.org/10.5194/egusphere-2026-6116
Preprint. Discussion started: 5 November 2026
© Author(s) 2026. CC BY 4.0 License.



936 Korver, M. C., Lehner, B., Cardille, J. A., and Carrea, L.: Surface water temperature
937 observations and ice phenology estimations for 1.4 million lakes globally, Remote Sens.
938 Environ., 308, 114164, https://doi.org/10.1016/j.rse.2024.114164, 2024.

939 Kropáček, J., Maussion, F., Chen, F., Hoerz, S., and Hochschild, V.: Analysis of ice phenology
940 of lakes on the Tibetan Plateau from MODIS data, The Cryosphere, 7, 287–301,
941 https://doi.org/10.5194/tc-7-287-2013, 2013.

942 L'Abée-Lund, J. H., Vøllestad, L. A., Brittain, J. E., Kvambekk, Å. S., and Solvang, T.:
943 Geographic variation and temporal trends in ice phenology in Norwegian lakes during the period
944 1890–2020, The Cryosphere, 15, 2333–2356, https://doi.org/10.5194/tc-15-2333-2021, 2021.

945 Lake George Association: An historical look at ice on Lake George, Lake George Association,
946 Lake George, New York, https://lakegeorgeassociation.org/science-protection/citizen-science/
947 historical-look-ice-lake-george, last access: 3 October 2026, 2026.

948 Latifovic, R. and Pouliot, D.: Analysis of climate change impacts on lake ice phenology in
949 Canada using the historical satellite data record, Remote Sens. Environ., 106, 492–507,
950 https://doi.org/10.1016/j.rse.2006.09.015, 2007.

951 Leppäranta, M.: Freezing of Lakes and the Evolution of Their Ice Cover, 2nd edn., Springer,
952 Cham, https://doi.org/10.1007/978-3-031-25605-9, 2023.

953 Magnuson, J. J., Robertson, D. M., Benson, B. J., Wynne, R. H., Livingstone, D. M., Arai, T.,
954 Assel, R. A., Barry, R. G., Card, V., Kuusisto, E., Granin, N. G., Prowse, T. D., Stewart, K. M.,
955 and Vuglinski, V. S.: Historical trends in lake and river ice cover in the Northern Hemisphere,
956 Science, 289, 1743–1746, https://doi.org/10.1126/science.289.5485.1743, 2000.

957 McCullagh, P., and Nelder, J. A. (1989): Generalized Linear Models, 2nd ed., Chapman & Hall,
958 London, UK, 511 pp. DOI: 10.1007/978-1-4899-3242-6.

959 McNulty, S.: Lake ice surveys, 1874–2022, Adirondack Long-Term Ecological Monitoring
960 Program Project No. 8, Adirondack Ecological Center, State University of New York College of
961 Environmental Science and Forestry, Newcomb, New York, Environmental Data Initiative, ver.
962 3, https://doi.org/10.6073/pasta/bf65ecb5ffbf2d53986997a255e5901f, 2022.

https://doi.org/10.5194/egusphere-2026-6116
Preprint. Discussion started: 5 November 2026
© Author(s) 2026. CC BY 4.0 License.



963 Muñoz-Sabater, J., Dutra, E., Agustí-Panareda, A., Albergel, C., Arduini, G., Balsamo, G.,
964 Boussetta, S., Choulga, M., Harrigan, S., Hersbach, H., Martens, B., Miralles, D. G., Piles, M.,
965 Rodríguez-Fernández, N. J., Zsoter, E., Buontempo, C., and Thépaut, J.-N.: ERA5-Land: a state-
966 of-the-art global reanalysis dataset for land applications, Earth Syst. Sci. Data, 13, 4349–4383,
967 https://doi.org/10.5194/essd-13-4349-2021, 2021.

968 Murfitt, J. and Duguay, C. R.: Assessing the performance of methods for monitoring ice
969 phenology of the world's largest High Arctic lake using high-density time series analysis of
970 Sentinel-1 data, Remote Sens., 12, 382, https://doi.org/10.3390/rs12030382, 2020.

971 Murfitt, J. and Duguay, C. R.: 50 years of lake ice research from active microwave remote
972 sensing: progress and prospects, Remote Sens. Environ., 264, 112616,
973 https://doi.org/10.1016/j.rse.2021.112616, 2021.

974 Murfitt, J., Duguay, C., Picard, G., and Lemmetyinen, J.: Forward modelling of synthetic-
975 aperture radar (SAR) backscatter during lake ice melt conditions using the Snow Microwave
976 Radiative Transfer (SMRT) model, The Cryosphere, 18, 869–888, https://doi.org/10.5194/tc-18-
977 869-2024, 2024.

978 Pekel, J.-F., Cottam, A., Gorelick, N., and Belward, A. S.: High-resolution mapping of global
979 surface water and its long-term changes, Nature, 540, 418–422,
980 https://doi.org/10.1038/nature20584, 2016.

981 Rabiner, L. R.: A tutorial on hidden Markov models and selected applications in speech
982 recognition, Proc. IEEE, 77, 257–286, https://doi.org/10.1109/5.18626, 1989.

983 Roberts, D. R., Bahn, V., Ciuti, S., Boyce, M. S., Elith, J., Guillera-Arroita, G., Hauenstein, S.,
984 Lahoz-Monfort, J. J., Schröder, B., Thuiller, W., Warton, D. I., Wintle, B. A., Hartig, F., and
985 Dormann, C. F.: Cross-validation strategies for data with temporal, spatial, hierarchical, or
986 phylogenetic structure, Ecography, 40, 913–929, https://doi.org/10.1111/ecog.02881, 2017.

987 Sharma, S., Blagrave, K., Magnuson, J. J., O'Reilly, C. M., Oliver, S., Batt, R. D., Magee, M. R.,
988 Straile, D., Weyhenmeyer, G. A., Winslow, L., and Woolway, R. I.: Widespread loss of lake ice
989 around the Northern Hemisphere in a warming world, Nat. Clim. Change, 9, 227–231,
990 https://doi.org/10.1038/s41558-018-0393-5, 2019.

https://doi.org/10.5194/egusphere-2026-6116
Preprint. Discussion started: 5 November 2026
© Author(s) 2026. CC BY 4.0 License.

Sharma, S., Filazzola, A., Nguyen, T., Imrit, M. A., Blagrave, K., Bouffard, D., Daly, J., Feldman, H., Feldsine, N., Hendricks-Franssen, H.-J., Granin, N., Hecock, R., L'Abée-Lund, J. H., Hopkins, E., Howk, N., Iacono, M., Knoll, L. B., Korhonen, J., Malmquist, H. J., Marszelewski, W., Matsuzaki, S.-I. S., Miyabara, Y., Miyasaka, K., Mills, A., Olson, L., Peters, T. W., Richardson, D. C., Robertson, D. M., Rudstam, L., Wain, D., Waterfield, H., Weyhenmeyer, G. A., Wiltse, B., Yao, H., Zhdanov, A., and Magnuson, J. J.: Long-term ice phenology records spanning up to 578 years for 78 lakes around the Northern Hemisphere, Sci. Data, 9, 318, https://doi.org/10.1038/s41597-022-01391-6, 2022.

Shuter, B. J., Minns, C. K., and Fung, S. R.: Empirical models for forecasting changes in the phenology of ice cover for Canadian lakes, Can. J. Fish. Aquat. Sci., 70, 982–991, https://doi.org/10.1139/cjfas-2012-0437, 2013.

Skoglund, S. K., Bah, A. R., Norouzi, H., Weathers, K. C., Ewing, H. A., Steele, B. G., and Bacon, L. C.: Approximation of ice phenology of Maine lakes using Aqua MODIS surface temperature data, Ecosphere, 15, e70000, https://doi.org/10.1002/ecs2.70000, 2024.

Sobiech, J. and Dierking, W.: Observing lake- and river-ice decay with SAR: advantages and limitations of the unsupervised k-means classification approach, Ann. Glaciol., 54, 65–72, 2013.

Stager, J. C., Wiltse, B., and Murphy, S.: Once and future changes in climate and phenology within the Adirondack uplands (New York, USA), PLOS Clim., 1, e0000047, https://doi.org/10.1371/journal.pclm.0000047, 2022.

Surdu, C. M., Duguay, C. R., Brown, L. C., and Fernández Prieto, D.: Response of ice cover on shallow lakes of the North Slope of Alaska to contemporary climate conditions (1950–2011): radar remote-sensing and numerical modeling data analysis, The Cryosphere, 8, 167–180, https://doi.org/10.5194/tc-8-167-2014, 2014.

Surdu, C. M., Duguay, C. R., and Fernández Prieto, D.: Evidence of recent changes in the ice regime of lakes in the Canadian High Arctic from spaceborne satellite observations, The Cryosphere, 10, 941–960, https://doi.org/10.5194/tc-10-941-2016, 2016.

https://doi.org/10.5194/egusphere-2026-6116
Preprint. Discussion started: 5 November 2026
© Author(s) 2026. CC BY 4.0 License.

Thornton, M. M., Shrestha, R., Wei, Y., Thornton, P. E., and Kao, S.-C.: Daymet: Daily Surface Weather Data on a 1-km Grid for North America, Version 4, ORNL DAAC, Oak Ridge, Tennessee, https://doi.org/10.3334/ORNLDAAC/1840, 2020.

Tom, M., Aguilar, R., Imhof, P., Leinss, S., Baltsavias, E., and Schindler, K.: Lake ice detection from Sentinel-1 SAR with deep learning, ISPRS Ann. Photogramm. Remote Sens. Spatial Inf. Sci., V-3-2020, 409–416, https://doi.org/10.5194/isprs-annals-V-3-2020-409-2020, 2020.

Tong, J., Lin, Y., Fan, C., Liu, K., Chen, T., Zeng, F., Zhan, P., Ke, L., Gao, Y., and Song, C.: Fine-scale monitoring of lake ice phenology by synthesizing remote sensed and climatologic features based on high-resolution satellite constellation and modeling, Sci. Total Environ., 912, 169002, https://doi.org/10.1016/j.scitotenv.2023.169002, 2024.

Torres, R., Snoeij, P., Geudtner, D., Bibby, D., Davidson, M., Attema, E., Potin, P., Rommen, B., Floury, N., Brown, M., Navas Traver, I., Deghaye, P., Duesmann, B., Rosich, B., Miranda, N., Bruno, C., L'Abbate, M., Croci, R., Pietropaolo, A., Huchler, M., and Rostan, F.: GMES Sentinel-1 mission, Remote Sens. Environ., 120, 9–24, https://doi.org/10.1016/j.rse.2011.05.028, 2012.

Ulaby, F. T., Moore, R. K., and Fung, A. K. (1986). Microwave Remote Sensing: Active and Passive. Volume III: From Theory to Applications. Artech House.

Viterbi, A. J.: Error bounds for convolutional codes and an asymptotically optimum decoding algorithm, IEEE Trans. Inf. Theory, 13, 260–269, https://doi.org/10.1109/TIT.1967.1054010, 1967.

Weber, H., Riffler, M., Nõges, T., and Wunderle, S.: Lake ice phenology from AVHRR data for European lakes: an automated two-step extraction method, Remote Sens. Environ., 174, 329–340, 2016.

Williams, G. P.: Correlating freeze-up and break-up with weather conditions, Can. Geotech. J., 2, 313–326, https://doi.org/10.1139/t65-040, 1965.

Woolway, R. I., Kraemer, B. M., Lenters, J. D., Merchant, C. J., O'Reilly, C. M., and Sharma, S.: Global lake responses to climate change, Nat. Rev. Earth Environ., 1, 388–403, 2020.

https://doi.org/10.5194/egusphere-2026-6116
Preprint. Discussion started: 5 November 2026
© Author(s) 2026. CC BY 4.0 License.



1044 Wu, Y., Duguay, C. R., and Xu, L.: Assessment of machine learning classifiers for global lake
1045 ice cover mapping from MODIS TOA reflectance data, Remote Sens. Environ., 253, 112206,
1046 https://doi.org/10.1016/j.rse.2020.112206, 2021.

1047 Zhang, S. and Pavelsky, T. M.: Remote sensing of lake ice phenology across a range of lake
1048 sizes, Maine, USA, Remote Sens., 11, 1718, https://doi.org/10.3390/rs11141718, 2019.